Valence band effective-mass Hamiltonians for the group-III nitrides from quasiparticle self-consistent *GW* band structures

Atchara Punya and Walter R. L. Lambrecht
Department of Physics, Case Western Reserve University, Cleveland, Ohio 44106-7079, USA
(Received 27 April 2012; published 29 May 2012)

We present band gaps, electron effective masses, and valence band effective-mass Hamiltonian parameters as well as strain deformation potentials of the crystal field splittings for AlN, GaN, and InN obtained from quasiparticle self-consistent *GW* calculations. Excellent agreement is obtained with experimental data for the crystal field and spin-orbit coupling splittings of bulk AlN and GaN. For InN, the discrepancy on the crystal field splitting is likely due to the residual strain in InN thin films from which that experimental value was extracted. We obtain a negative spin-orbit splitting for InN, which is plausible in view of the stronger negative contribution of In-4*d* in InN than Ga-3*d* in GaN. The inverse effective-mass parameters A_i agree well with previous G_0W_0 calculations except for A_6. We find that the A_6 parameter describing the band dispersion in directions intermediate between parallel and perpendicular to the basal plane is not well described by the quasicubic approximation. Good agreement with the most reliable experimental data is obtained for hole effective-mass parameters in AlN and GaN, extracted from exciton binding energies and their fine structure. For InN and GaN, the spin-splittings of the bands in the plane due to spin-orbit coupling requires the inclusion of linear in **k** and spin terms.

DOI: 10.1103/PhysRevB.85.195147 PACS number(s): 71.20.Nr, 71.15.Mb

I. INTRODUCTION

The group-III nitride semiconductors AlN, GaN, and InN are important for a variety of optoelectronic and electronic applications. To model electronic states, optical properties, and transport in quantum well heterostructures, nanowires, and nanoparticles of these materials, one often uses a description in terms of a six-band effective-mass Hamiltonian describing the valence band maximum manifold of nearly degenerate states near the center of the Brillouin zone. Within the envelope function approximation, the states of these nanostructures are described as a linear combination of products of slowly varying envelope functions and the Bloch functions of the crystal near the valence band maximum. This effective-mass Hamiltonian approach is also used in the theory of excitons and shallow acceptors. The effective-mass Hamiltonian for semiconductors with zincblende structure was introduced by Luttinger and Kohn.[1,2] Its form is determined by the theory of invariants. Its generalization for wurtzite crystals was introduced by Rashba, Sheka, and Pikus (RSP).[3–7]

The parameters for these effective-mass Hamiltonians include inverse effective mass parameters, describing all the terms of order k^2, crystal field and spin-orbit splittings at Γ and some linear in k terms. Strain dependent terms are added to the energy splittings. Several previous works have fitted these parameters to first-principles band structure results.[8–10] Because there were significant discrepancies on these parameters from different groups, and validation of these parameters by experimental methods is indirect, some efforts were made to arrive at a recommended set of values.[11,12] Recently, there has been a resurgence of interest[13–15] in improving these valence band parameters because more accurate band structure methods have become available, going beyond the local density approximation used in the work of the 90s. Among the group-III nitrides, InN requires perhaps the most important revisions because its band gap is now accepted[16,17] to be 0.7 eV while it was long believed to be about 1.89 eV.[18]

Rinke *et al.*[13] used G_0W_0 quasiparticle band structures starting from optimized effective potential exact exchange + LDA correlation, but focused on the fit only very near the Γ point. de Carvalho *et al.*[15] use G_0W_0 starting from hybrid functional HSE calculations. Svane *et al.*[14] used quasiparticle self-consistent *GW* calculations, very similar to the calculations reported here, but did not extract effective-mass Hamiltonian parameters. It focused only on the effective masses and splittings.

In this paper, we revisit the problem once more with several differences to be mentioned from the previous work. First, we use the quasiparticle self-consistent *GW* (QS*GW*) method developed by van Schilfgaarde *et al.*[19,20] This method has a distinct advantage for determining the fine structure of the band structure, such as effective masses. In fact, its use of a linearized muffin-tin orbital basis set allows for a real space representation of the *GW* self-energy. This can then be Fourier transformed back to k space on a much finer mesh than the k mesh for which the *GW* calculations need to be carried out. This is important to extract reliable effective masses.

Second, we have re-evaluated the process for most reliably extracting the effective-mass Hamiltonian parameters. While some derive directly from the effective masses without spin-orbit coupling in or perpendicular to the basal plane, some of the parameters such as A_6 required fitting the band structures in an intermediate k-space direction if one does not wish to rely on quasicubic approximations. The linear in k-parameter A_7 also requires careful evaluation of the band anticrossing behavior. These aspects will be discussed in detail below. The determination of the spin-orbit and crystal field splittings and the validity of the quasicubic approximation for the former also requires some discussion. We show that in GaN and InN, relativistic terms linear in **k** need to be included to properly describe the spin splittings.

Finally, the crystal field splitting at Γ is particularly sensitive both to the GW corrections to the band structure and to the crystal structure, such as c/a ratio. This means in practice it is dependent on uniaxial strain. We therefore think it is essential to include a description of the latter in terms of deformation potentials.

As our main results, we mention that we find a crystal field splitting in GaN much closer to experiment than in previous work. Secondly, we find a negative spin-orbit splitting for InN. We also discuss the recent experimental work on AlN band parameters in view of our results.[21,22]

II. FIRST-PRINCIPLES COMPUTATIONAL METHOD

We use the density functional theory[23,24] in the local density approximation to determine the equilibrium crystal structure parameters. The full-potential linearized muffin-tin orbital method[25,26] is used to solve the Kohn-Sham equation.

The quasiparticle band structures are calculated using the quasiparticle self-consistent GW approach (QSGW) as developed by van Schilfgaarde and Kotani.[19,20] As is well known, the GW method originally proposed by Hedin[27] uses a product of the one-electron Green's function G and the screened Coulomb interaction W as first approximation for the quasiparticle self-energy. Within the random phase approximation, the screening polarizability is itself derived from the independent particle Green's function G_0 so that the self-energy, schematically written as $\Sigma = iG_0W_0$, can be viewed as a functional of G_0. A new nonlocal exchange correlation potential can then be extracted from the energy dependent Σ and defines hence a new independent particle Hamiltonian as the starting point for a new G_0. The QSGW method consists of iterating this process to convergence. It provides in a sense the best one-electron independent particle Hamiltonian so that the quasiparticle shift from it is minimized. At convergence, the quasiparticle Hamiltonian and the Kohn-Sham Hamiltonian have the same eigenvalues. Although we start from LDA, the final QSGW eigenvalues are independent of this approximation.

In practice, other details of the GW implementation used here set it apart from other recent calculations for the nitrides, mentioned in the introduction. It is implemented in the FP-LMTO method and uses a mixed basis set of plane waves and LMTO product basis functions for all two electron operators, such as the Coulomb interaction, the polarizability, and the self-energy operator. Details can be found in Ref. 20, and its performance for a wide variety of semiconductors is shown to be excellent in Ref. 19. More specifically, it slightly overestimates the gaps because of the underestimation of the screening by the random phase approximation but agrees to better than 0.1 eV for all known semiconductors after we scale the GW correction by a factor 0.8. This correction factor is included in the calculations here.

Some specific details of our calculations follow. We use a double (κ, R_{sm}) basis set consisting of $spdf$ and spd functions for the first and second set of group-III and N atoms. In addition we add $3d$ and $4d$ local orbitals of Ga and In atoms, and also spd floating orbitals. Here, κ is the smoothed Hankel function decay constant and R_{sm} is the smoothing radius. We use a GW k-point set of $4 \times 4 \times 4$ for AlN and GaN. In the case of InN, we found the results to be particularly sensitive to the k-point convergence and therefore used $6 \times 6 \times 4$. The self-energy is approximated by a diagonal approximation above a certain cutoff energy, as discussed in Kotani *et al.*[20] We choose this parameter to be 2 Ryd in GaN, AlN, and InN. Spin-orbit coupling is added independently of the GW self-energy in the end.

III. EFFECTIVE-MASS HAMILTONIAN AND PROCEDURE FOR EXTRACTING ITS PARAMETERS

The effective-mass Hamiltonian can be described in terms of the operators for $L = 1$ angular momentum representing the basis states of the threefold degenerate valence band maximum (VBM) at Γ without spin-orbit coupling, the Pauli matrices, representing the spin, the wave vector $\mathbf{k}$, and the strain tensor ϵ. The only allowed terms are those up to terms of second order in any of these quantities whose combination has the A_1 symmetry. In wurtzite, this Hamiltonian is described by:

$$
\begin{aligned}
H = {} & \Delta_1 L_z^2 + \Delta_2 L_z \sigma_z + \sqrt{2}\Delta_3 (L_+\sigma_- + L_-\sigma_+) + \left(A_1 + A_3 L_z^2\right)k_z^2 + \left(A_2 + A_4 L_x^2\right)\left(k_x^2 + k_y^2\right) - A_5(L_+^2 k_-^2 + L_-^2 k_+^2) \\
& - 2iA_6 k_z(\{L_z, L_+\}k_- - \{L_z, L_-\}k_+) + A_7(k_- L_+ + k_+ L_-) + \left(\alpha_1 + \alpha_3 L_z^2\right)(\sigma_+ k_- + \sigma_- k_+) + \alpha_2(L_+^2 k_- \sigma_- + L_-^2 k_+ \sigma_+) \\
& + 2\alpha_4 \sigma_z(\{L_z, L_+\}k_- + \{L_z, L_+\}k_+) + 2i\alpha_5 k_z(\{L_z, L_+\}\sigma_- - \{L_z, L_-\}\sigma_+) + \left(D_1 + D_3 L_z^2\right)\epsilon_{zz} + \left(D_2 + D_4 L_z^2\right)\epsilon_\perp \\
& - D_5(L_+^2 \epsilon_- + L_-^2 \epsilon_+) - 2iD_6(\{L_z, L_+\}\epsilon_{-z} - \{L_z, L_-\}\epsilon_{+z}).
\end{aligned} \tag{1}
$$

Here, $\{L_z, L_-\} = \frac{1}{2}(L_z L_- + L_- L_z)$ is the symmetrized product, $L_\pm = \frac{1}{\sqrt{2}}(\pm iL_x - L_y)$, $\sigma_\pm = \frac{1}{2}(\pm i\sigma_x - \sigma_y)$, $k_\pm = k_x \pm ik_y$, $k_\perp^2 = k_x^2 + k_y^2$, $\epsilon_\perp = \epsilon_{xx} + \epsilon_{yy}$, $\epsilon_{\pm z} = \epsilon_{xz} \pm i\epsilon_{yz}$, and $\epsilon_\pm = \epsilon_{xx} - \epsilon_{yy} \pm 2i\epsilon_{xy}$. The parameters Δ_1, Δ_2, Δ_3 are the crystal field splitting and spin-orbit coupling parameters. The A_1–A_6 are inverse effective-mass type parameters and the A_7 is a nonrelativistic (spin-independent) linear in $\mathbf{k}$ term. Relativistic terms linear in $\mathbf{k}$ and spin are described by the α_1–α_5 terms. The parameters A_1–A_5 are directly related to the hole masses in the plane and perpendicular to the plane by means of

$$
\begin{aligned}
-(m_{hh}^{\parallel})^{-1} &= A_1 + A_3 \\
-(m_{sh}^{\parallel})^{-1} &= A_1 \\
-(m_{hh}^{\perp})^{-1} &= A_2 + A_4 + A_5 \\
-(m_{lh}^{\perp})^{-1} &= A_2 + A_4 - A_5 \\
-(m_{sh}^{\perp})^{-1} &= A_2.
\end{aligned} \tag{2}
$$

The parameter A_6 only affects the bands in directions intermediate between the plane and perpendicular to it. While in Kim *et al.*[10] these were obtained by means of the quasicubic approximation from the previous parameters, we here determine it directly by fitting the bands in an intermediate direction. We will show explicitly that the quasicubic approximation is not sufficient.

As described in detail in Kim *et al.*,[10] the A_7 parameter is related to the avoided band crossing of the light hole and crystal field split-off band. When it is set to zero the bands cross. The split-off band then has a large effective hole mass. When A_7 is switched on, the crossing is lifted. The light hole and split-off hole masses are changed respectively by

$$\pm 2A_7^2/|\Delta_1|. \tag{3}$$

The parameter A_7 is determined by fitting the nonparabolic shapes of the bands near this crossing directly by manually adjusting A_7 until good agreement is obtained.

The crystal field splitting parameter at Γ is directly obtained from the calculation without spin-orbit coupling. It is defined as the difference $\Delta_1 = E(\Gamma_5) - E(\Gamma_1)$ between the doublet and singlet of the VBM. When spin-orbit coupling is included the Γ_5 state splits into a Γ_9 and Γ_7 state. The latter can then interact with the nearby crystal field split-off state Γ_1 because in double group notation, Γ_1 becomes Γ_7. This leads to the eigenvalues given by

$$\begin{aligned} E_9 &= \Delta_1 + \Delta_2 \\ E_{7\pm} &= \frac{\Delta_1 - \Delta_2}{2} \pm \sqrt{\left(\frac{\Delta_1 - \Delta_2}{2}\right)^2 + 2\Delta_3^2}. \end{aligned} \tag{4}$$

The two splittings allow us to determine the parameters Δ_2 and Δ_3. We already know Δ_1 or assume it is not changed by spin-orbit coupling. While in some other cases, this procedure may lead to difficulties, (it may lead to an imaginary Δ_3) it works fine for all nitrides considered here. On the other hand, one may assume a quasicubic approximation for spin-orbit coupling $\Delta_2 = \Delta_3$. In that case, there are only two parameters determining the two energy splittings and they can directly be determined.

The crystal field splitting $\Delta_c = E(\Gamma_5) - E(\Gamma_1)$ is sensitive to uniaxial strain. For a uniaxial volume conserving (traceless) strain in the z direction, $\epsilon_{xx} = \epsilon_{yy} = -\epsilon_{zz}/2$. Eq. (1) then gives

$$\Delta_c = \Delta_1 + (D_3 - D_4)\epsilon_{zz}. \tag{5}$$

On the other hand, for an isotropic volume change, the strain tensor is $\epsilon_{xx} = \epsilon_{yy} = \epsilon_{zz} = \epsilon/3$ with $\epsilon = dV/V$. In that case,

$$\Delta_c = \Delta_1 + (D_3 + 2D_4)\frac{dV}{V}. \tag{6}$$

By fitting Δ_1 extracted from the band structure for isotropic and uniaxial strains, we can determine both D_3 and D_4. In the quasicubic approximation $D_3 = -2D_4$, there would be no isotropic strain change in crystal field splitting, and the uniaxial effect reduces to $\frac{3}{2}D_3\epsilon_{zz}$. Thin films are often under biaxial strain, which has both a uniaxial and isotropic component. By providing both D_3 and D_4, the change in crystal field splitting can easily be obtained for any biaxial strain situation that might occur depending on growth conditions, temperature, and film thickness. The parameters D_1 and D_2 only lead to shifts of the bands and were not determined. The parameters D_5 and D_6 only enter when strains breaking the hexagonal symmetry are considered. We did not determine them here because they are of less interest for thin films. Finally, we also determine the band gap hydrostatic strain deformation potentials as

$$a_v = dE_g/d\ln V. \tag{7}$$

IV. RESULTS

A. Band structure parameters

The structural parameters obtained from our LDA optimization are in good agreement with experiments and previous calculations and are given in Table I for reference. For InN no experimental value is available for the u parameter, but our value agrees well with that of de Carvalho *et al.*,[15] 0.378, Svane *et al.*,[14] 0.379, and Rinke *et al.*,[13] 0.380.

The band structures near the VBM without spin-orbit coupling are shown for AlN, GaN, and InN in Fig. 1 for **k** along the c axis ($k_\parallel$) and in the plane ($k_\perp$). The solid lines indicate the fits by means of the effective-mass Hamiltonian. Separately, in Fig. 2 we show the bands for a direction between the two at an angle of 45° illustrating the inadequacy of using the quasicubic approximation for A_6.

The band structures including spin-orbit coupling are shown in Fig. 3 together with the effective-mass Hamiltonian results. These include the same parameters as before plus the spin-orbit splitting parameters at Γ. It shows that now the bands become spin-split in the plane. Along the c axis, they are still degenerate because by time reversal $\psi_{k_z\sigma} = \psi_{-k_z-\sigma}$, and by the glide mirror plane perpendicular to the c axis $\psi_{k_z\sigma} = \psi_{-k_z\sigma}$. Hence there is a Kramer's degeneracy. In order to fully adjust

TABLE I. Lattice parameters (Å) a, c, c/a, u.

	AlN		GaN		InN	
	LDA	Expt.	LDA	Expt.	LDA	Expt.
a	3.112	3.11[a]	3.157	3.19[a]	3.508	3.54[b]
c	4.975	4.978[a]	5.143	5.166–5.185[a]	5.666	5.718[a]
c/a	1.599	1.601[a]	1.629	1.627[a]	1.615	1.613[b]
u	0.382	0.382[a]	0.376	0.377[a]	0.380	

[a]Expt. from Schulz *et al.* (Ref. 28).
[b]Expt. from Ueno *et al.* (Ref. 29).

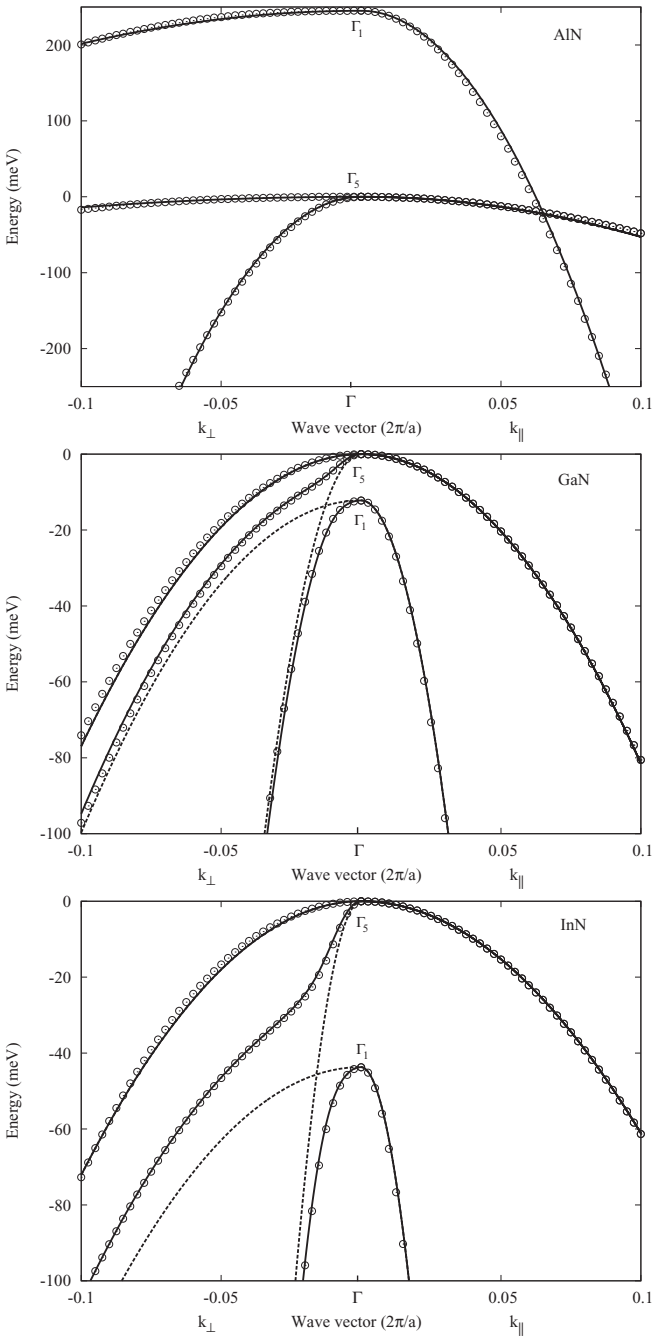

FIG. 1. Valence bands of AlN, GaN, and InN without spin-orbit coupling, dots represent QSGW results, full lines represent the RSP fits including A_7, dashed lines excluding A_7. The zero of energy is at the Γ_5 state.

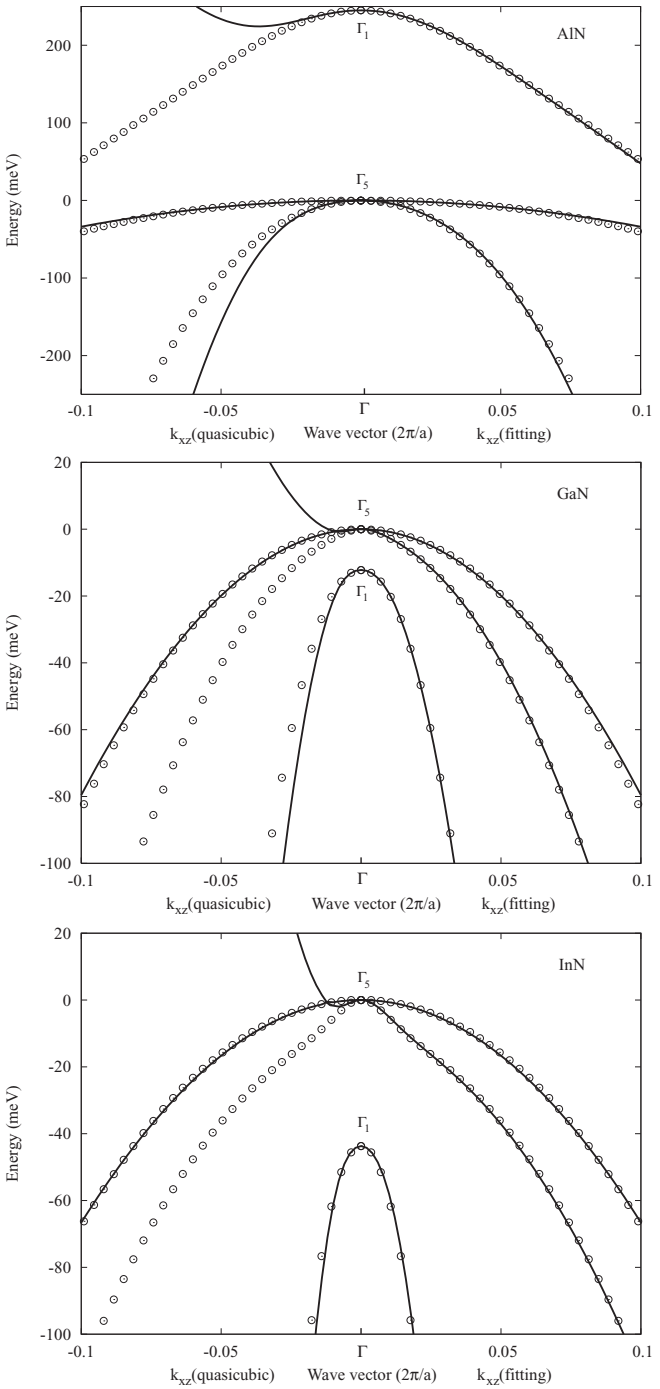

FIG. 2. Valence bands of AlN, GaN, and InN without spin-orbit coupling in the direction between in-plane and perpendicular to plane at angle 45°. Left hand side: using quasicubic approximation, right hand side: using manual fitting. The zero of energy is at the doubly degenerate Γ_5 state. Dots represent QSGW results, full lines represent the RSP fits.

the spin splittings in the plane, we also needed to add the small relativistic linear in $\mathbf{k}$,α terms, for GaN and InN. This is shown in Fig. 4. For AlN, we notice that along $k_\parallel$, the upper band crosses the second band but not the third band. This is because the upper band has Γ_7 symmetry along the line $\Delta = \Gamma - A$, the second band has Γ_9 symmetry, and the third band has Γ_7 symmetry. Bands of the same symmetry cannot cross because an interaction between the two avoids the crossing.

The parameters are summarized in Table II. Here we use $\Delta_{so}^{\parallel} = 3\Delta_2$, $\Delta_{so}^{\perp} = 3\Delta_3$. In the quasicubic approximation $\Delta_{so}^{\parallel} = \Delta_{so}^{\perp} = \Delta_{so}^{ZB}$, the latter being the value in the zincblende structure. Using this approximation, we can extract Δ_1 and Δ_2 directly from the two band splittings using Eq. (4).

Finally, we include the (spin-averaged) effective masses of the three separate valence band maxima, A, B, C when spin-orbit coupling is included as shown in Table III. Here, A means Γ_9, B means Γ_{7+}, and C means Γ_{7-}.

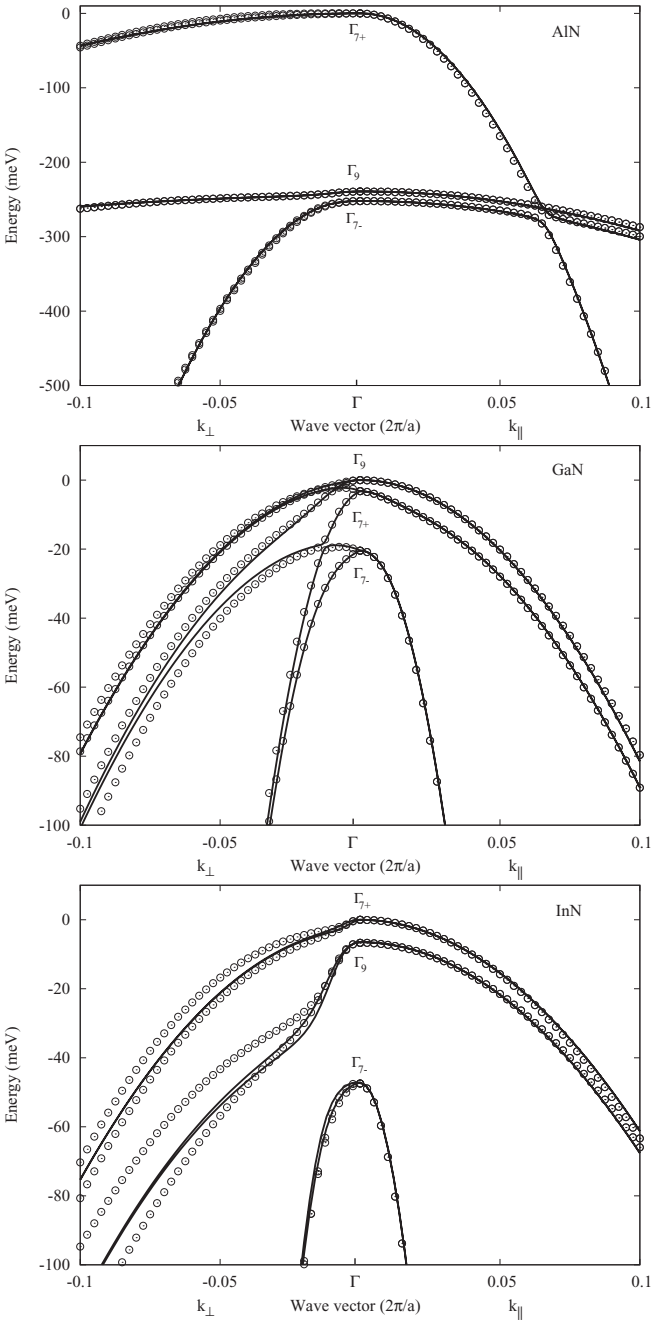

FIG. 3. Valence bands of AlN, GaN, and InN including spin-orbit couplings, but neglecting the α_i spin-dependent terms. The zero of energy is at the valence band maximum, which is Γ_9 in GaN, Γ_{7+} in AlN and InN. Dots represent QSGW results, full lines represent the RSP fits.

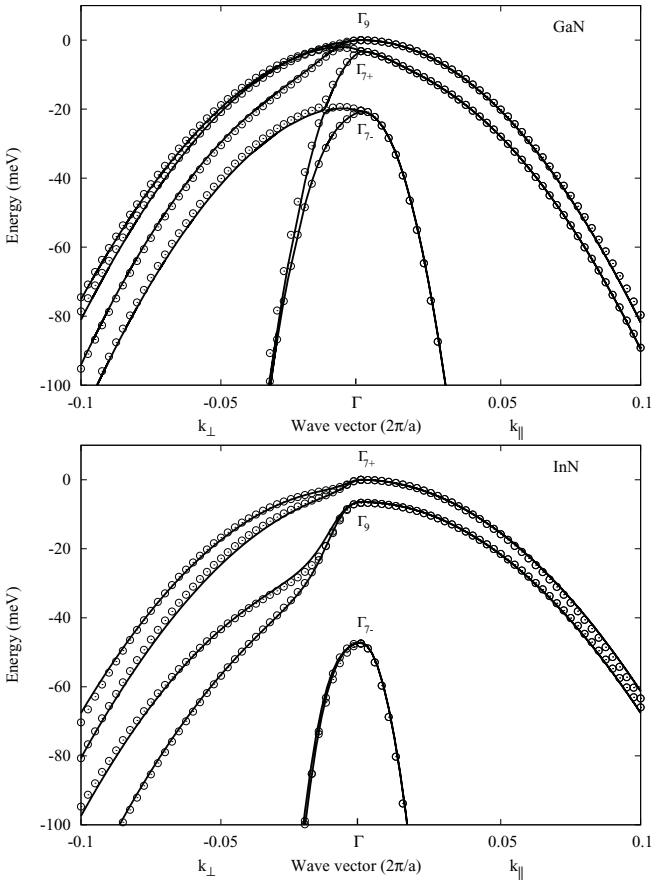

FIG. 4. Valence bands of GaN and InN including spin-orbit couplings and the additional α_i spin-dependent terms. The zero of energy is at the valence band maximum. Dots represent QSGW results, full lines represent the RSP fits.

V. DISCUSSION

The crystal field and spin-orbit coupling parameters are compared with other recent calculations and experimental data in Table IV. We note that the crystal field splitting is sensitive to strain. The experimental values quoted here for AlN are for bulk single crystals.[34,35] For GaN, they correspond to 500-μm-thick layers.[36] For InN, the only value we could find is for a rather thin film of only 670 nm on r-plane sapphire.[37] This value is likely to be influenced by some residual strain.

We can see in Table II that the QSGW values differ significantly from the LDA values for the deformation potentials. While for AlN and GaN the quasicubic approximation $D_3 + 2D_4 \approx 0$ are reasonably well obeyed, the deviation from quasicubic is significant for InN. The band gap deformation potentials are all negative. The decrease of the band gap with increasing lattice constant is the usual behavior in covalent semiconductors. Our values are comparable to those of Rinke *et al.*[13]: −9.8 eV for AlN, −7.6 for GaN, and −4.2 for InN.

We found the crystal field splitting of InN to be very sensitive to computational details. For example, using a smaller GW k-point set, we obtained a negative crystal field splitting of −14.8 meV. A small compressive strain along the c axis could easily reduce the crystal field splitting and even make it negative. This is accompanied by a significant change in the band structure as illustrated in Figs. 5 and 6. The valence band maximum in that case moves away from Γ due to the repulsion between the crystal field split-off and light hole band. We can see that this off-Γ valence band maximum persists up to a positive crystal field splitting of about 15 meV. Given the deformation potentials, we can see that uniaxial compressive strain of order 1–2% could cause the crystal field splitting to go from positive to negative and shift the valence band maximum away from Γ.

TABLE II. Band structure parameters: inverse masses (A_1–A_6) (in units $\hbar^2/2m_e$), energy splittings (Δ_1–Δ_3) (in meV), A_7 and α_i (in units $e^2/2$), band gap and deformation potentials (in eV). The value of $A_6, \Delta_1, \Delta_2, \Delta_3$ in parentheses are obtained in the quasicubic approximation. Electron effective masses (in units m_e). The hole masses correspond to the band structure without spin-orbit coupling. The hole masses obtained with A_7 from Eq. (3) are in parentheses.

parameter	AlN	GaN	InN
E_g	6.19	3.60	0.70
A_1	−4.05	−5.98	−15.7
A_2	−0.28	−0.58	−0.63
A_3	3.71	5.44	15.2
A_4	−1.71	−2.46	−7.10
A_5	1.90	2.53	7.14
A_6	−1.05(−2.75)	−1.55(−3.31)	−5.03(−9.45)
A_7	0	0.03	0.09
Δ_1	−245(−245)	12.2(18.2)	43.7(43.4)
$\Delta_{so}^{\parallel} = 3\Delta_2$	18.6(18.9)	11.7(5.4)	−9.5(−9.2)
$\Delta_{so}^{\perp} = 3\Delta_3$	22.5(18.9)	16.2(5.4)	−5.9(−9.2)
$m_e^{\parallel}$	0.32	0.20	0.09
Expt.	0.29–0.4[a]	0.20[b]	0.05–0.07[c]
$m_e^{\perp}$	0.31	0.22	0.09
$m_{hh}^{\parallel} = m_{lh}^{\parallel}$	2.94	1.85	2.00
$m_{sh}^{\parallel}$	0.25	0.17	0.06
$m_{hh}^{\perp}$	11.11	1.96	1.69
$m_{lh}^{\perp}$w/o A_7	0.26	0.18	0.07
$m_{lh}^{\perp}$ with A_7		0.30(0.28)	0.10(0.10)
$m_{sh}^{\perp}$w/o A_7	3.57	1.72	1.59
$m_{sh}^{\perp}$ with A_7		0.36(0.39)	0.17(0.18)
α_1		0.0028	−0.0095
α_2		0.0080	0.0135
α_3		−0.0030	0.0110
α_4		0.0028	0.0035
α_5		0	0
$D_3 - D_4$ (LDA)	6.04	5.43	2.70
$D_3 + 2D_4$(LDA)	0.23	−0.14	2.78
$D_3 - D_4$(QSGW)	14.3	4.71	2.98
$D_3 + 2D_4$(QSGW)	0.52	−0.04	−1.25
$a_v = dE_g/d\ln V$	−9.78	−8.41	−2.33

[a]Reference 30.
[b]Reference 12 and references therein.
[c]References 31 and 32.

TABLE III. Hole effective mass with spin-orbit coupling included. The masses obtained from directly fitting the effective-mass Hamiltonian bands near the Γ point are given in the first line for each material, the numbers in parentheses are obtained from second order perturbation theory as given in Eq. (10) in Kim *et al*. (Ref. 10). Only for GaN, a direct comparison to experimental values obtained from exciton binding energies is available.

	$m_A^{\parallel}$	$m_B^{\parallel}$	$m_C^{\parallel}$	$m_A^{\perp}$	$m_B^{\perp}$	$m_C^{\perp}$
AlN	2.94	0.25	2.83	0.56	3.53	0.46
	(2.94)	(0.25)	(2.89)	(0.50)	(3.53)	(0.50)
GaN	1.85	0.55	0.20	0.69	0.50	0.80
	(1.85)	(0.51)	(0.22)	(0.33)	(0.42)	(0.82)
[a]	1.76	0.419	0.299	0.349	0.512	0.676
InN	2.00	1.86	0.06	0.15	0.14	1.26
	(2.00)	(1.81)	(0.06)	(0.13)	(0.13)	(1.53)

[a]Expt. from Rodina *et al*. (Ref. 33).

TABLE IV. Comparison of the band gaps (in eV) and valence band splittings (in meV) to previous calculations and experiment.

		QSGW	Ref. 15	Ref. 13	Expt.
AlN	E_g	6.19	6.55	6.47	6.3
	Δ_1	−245	−260	−295	−230[a],−225[a]
	$\Delta_{so}^{\parallel}$	19	22		36[b]
	$\Delta_{so}^{\perp}$	22	22		
	$\Gamma_9 - \Gamma_{7+}$	−239.2	14.9		14[a], 25[b]
	$\Gamma_9 - \Gamma_{7-}$	12.9	−235.9		−218[a],−214[b]
GaN	E_g	3.60	3.85	3.24	3.5
	Δ_1	12	34	34	10[c]
	$\Delta_{so}^{\parallel}$	12	17		18.6[c]
	$\Delta_{so}^{\perp}$	16	20		16.5[c]
	$\Gamma_9 - \Gamma_{7+}$	3.2	8.7		7[c]
	$\Gamma_9 - \Gamma_{7-}$	20.4	49.3		23[c]
InN	E_g	0.70	0.76	0.67	0.65–0.8
	Δ_1	44	38	67	19-24[d]
	$\Delta_{so}^{\parallel}$	−9	11		
	$\Delta_{so}^{\perp}$	−6	20		
	$\Gamma_9 - \Gamma_{7+}$	−6.5	5.4		3[d]
	$\Gamma_9 - \Gamma_{7-}$	40.7	47.4		21[d]

[a]Chen *et al*. (Ref. 34).
[b]Silveira *et al*. (Ref. 35).
[c]B. Gil *et al*. (Ref. 36).
[d]Goldhahn *et al*. (Ref. 37).

Our crystal field splitting for GaN is in better agreement with experiment than previous results. It was already pointed out by Kim *et al*.[10] that this value was likely overestimated by LDA (or GGA) because the Γ_{1v} valence band is repelled by the Γ_{1c} conduction band and hence, an underestimate of the gap results in an overestimate of the crystal field splitting. Clearly it is extremely sensitive to computational details, since it depends on the precise computational details of the GW method as well as the crystal structure, which must be truly strain free.

We also note that we find here a negative value for the spin-orbit splitting in InN, in contrast to earlier reports.[13,15] We note that in order to ascertain the sign of the spin-orbit coupling we need to examine the symmetry of the valence band states at Γ. Whereas the Γ_{7+} state has a small p_z component in its wave function, the Γ_9 has no p_z component by symmetry. We find definitely a $\Gamma_{7+} > \Gamma_9 > \Gamma_{7-}$ ordering. The negative spin-orbit splitting arises from the contribution of the In-4d orbitals to the effective spin-orbit splitting. Because the latter lie below the VBM they give rise to a negative contribution. This is well known to also be the case for ZnO.[38] In that case, the Zn-3d states are closer to the VBM. The value in GaN is already small due to the coupling with the Ga-3d and the small value of the N-2p atomic spin-orbit coupling which tend to compensate each other. One may expect the In-4d contribution to be larger in magnitude because In is a heavier atom. Therefore it is plausible that it becomes negative in InN.

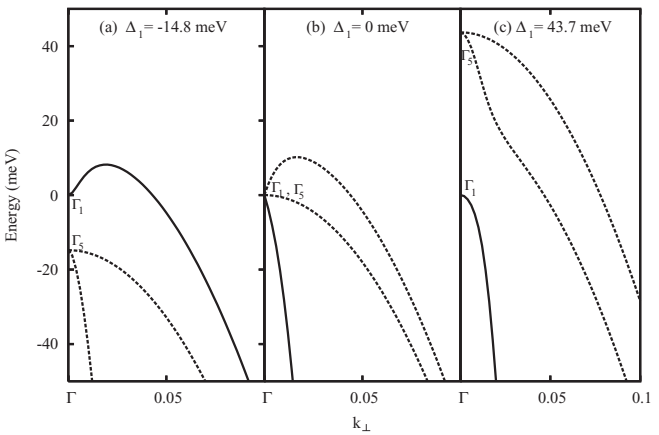

FIG. 5. Valence bands of InN without spin-orbit coupling calculated from the effective-mass Hamiltonian (a) $\Delta_1 < 0$, (b) $\Delta_1 = 0$, (c) $\Delta_1 > 0$.

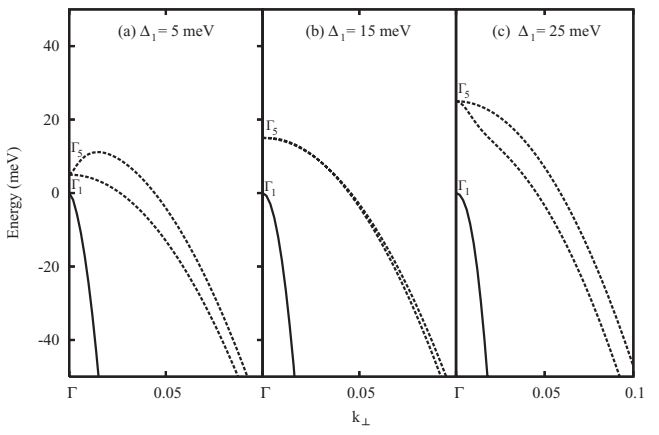

FIG. 6. Valence bands of InN without spin-orbit coupling calculated from the effective-mass Hamiltonian, with various positive crystal field splitting.

Next, we compare the A_i parameters to previous work. Our results agree quite closely with those of Rinke *et al.*[13] except for the parameter A_6. As we mentioned earlier, this parameter requires some care to extract it. Rinke *et al.*[13] used an automatic fitting to calculated band structures on a mesh of points near Γ but restricted themselves to obtaining a fit only very near Γ. In contrast, our fitted band structures can be seen to fit very well over a rather extended region of k space and down to energies of order 100 meV below the VBM. This is important if one wants to apply the method for calculating shallow acceptors which have binding energies of this order of magnitude.

For AlN, Gil[21,22] recently reviewed how well the A_1,A_2 parameters fit the experimental data on the $1s$-$2s$ exciton splitting. In order to obtain a good fit, he found it is important to also include the anisotropy of the dielectric constants. The best fit corresponded to $A_1 = -3.95$ and $A_2 = -0.27$, in excellent agreement with our calculated values. The reason why only the A_1 and A_2 enter here is that in AlN, the VBM has Γ_1 symmetry and thus the split-off hole band lies above the usual heavy and light hole. From Eq. (2) we can see that then A_1 and A_2 are respectively the inverse masses for the directions parallel and perpendicular to the c axis. They enter the reduced mass of the excitons that goes into the equation for the exciton binding energy.

For GaN, the most complete set of valence band effective masses is obtained again from a study of the exciton fine structure by Rodina *et al.*[33] Their values are included in the above Table III for comparison. For InN, no reliable experimental data on the hole masses are available to the best of our knowledge.

The conduction band effective masses for AlN, GaN, and InN all agree well with experimental data and are only slightly anisotropic. The experimental values included in Table II do not resolve the anisotropy.

VI. CONCLUSION

The parameters of the valence band effective-mass Hamiltonians were determined for AlN, GaN, and InN from quasiparticle self-consistent GW band structures. Because the crystal field splitting is strongly dependent on strain, the relevant strain deformation potentials are also determined. Good agreement is obtained with experiment for the band gaps and valence band maximum splittings at Γ in AlN and GaN. Our calculated effective masses, including spin-orbit coupling effects also agree well with those extracted from exciton fine structure in AlN and GaN. For InN, it is concluded that experimental data for strain free material is not yet available. We find the spin-orbit coupling parameter in InN to be negative and show that the band structure will be strongly dependent on strain. For both GaN and InN relativistic terms linear in **k** and spin need to be included to fully account for the spin splitting of the bands away from Γ.

ACKNOWLEDGMENTS

This work was supported by the National Science Foundation under Grant No. DMR-1104595 and made use of the High Performance Computing Resource in the Core Facility for Advanced Research Computing at Case Western Reserve University.

[1] J. M. Luttinger and W. Kohn, Phys. Rev. **97**, 869 (1955).
[2] J. M. Luttinger, Phys. Rev. **102**, 1030 (1956).
[3] G. L. Bir and G. E. Pikus, *Symmetry and Strain-Induced Effects in Semiconductors* (Wiley, New York, 1974).
[4] Y. M. Sirenko, J.-B. Jeon, K. W. Kim, M. A. Littlejohn, and M. A. Stroscio, Phys. Rev. B **53**, 1997 (1996).
[5] E. I. Rashba, Fiz. Tverd. Tela **1**, 407 (1959) [Sov. Phys. Solid State **1**, 368 (1959)] .
[6] E. I. Rashba and V. I. Sheka, Fiz. Tverd. Tela **1**, 162 (1959).
[7] G. E. Pikus, Zh. Eksp. Teor. Fiz. **41**, 1258 (1961) [Sov. Phys. JETP **14**, 898 (1962)].
[8] M. Suzuki, T. Uenoyama, and A. Yanase, Phys. Rev. B **52**, 8132 (1995).
[9] J. A. Majewski, M. Städle, and P. Vogl, in *III-V Nitrides, MRS Symposia Proceedings No. 449*, edited by F. A. Ponce, T. D. Moustakas, I. Akasaki, and B. A. Monemar (Materials Research Society, Pittsburgh, 1997), p. 887.
[10] K. Kim, W. R. L. Lambrecht, B. Segall, and M. van Schilfgaarde, Phys. Rev. B **56**, 7363 (1997).
[11] I. Vurgaftman, J. R. Meyer, and L. R. Ram-Mohan, J. Appl. Phys. **89**, 5815 (2001).
[12] I. Vurgaftman and J. R. Meyer, J. Appl. Phys. **94**, 3675 (2003).
[13] P. Rinke, M. Winkelnkemper, A. Qteish, D. Bimberg, J. Neugebauer, and M. Scheffler, Phys. Rev. B **77**, 075202 (2008).
[14] A. Svane, N. E. Christensen, I. Gorczyca, M. van Schilfgaarde, A. N. Chantis, and T. Kotani, Phys. Rev. B **82**, 115102 (2010).
[15] L. C. de Carvalho, A. Schleife, and F. Bechstedt, Phys. Rev. B **84**, 195105 (2011).
[16] V. Davydov, A. Klochikhin, R. Seisyan, V. Emtsev, S. Ivanov, F. Bechstedt, J. Furthmller, H. Harima, A. Mudryi, J. Aderhold, O. Semchinova, and J. Graul, Phys. Status Solidi B **229**, r1 (2002).
[17] J. Wu, W. Walukiewicz, K. M. Yu, J. W. A. III, E. E. Haller, H. Lu, W. J. Schaff, Y. Saito, and Y. Nanishi, Appl. Phys. Lett. **80**, 3967 (2002).
[18] T. L. Tansley and C. P. Foley, J. Appl. Phys. **59**, 3241 (1986).
[19] M. van Schilfgaarde, T. Kotani, and S. Faleev, Phys. Rev. Lett. **96**, 226402 (2006).
[20] T. Kotani, M. van Schilfgaarde, and S. V. Faleev, Phys. Rev. B **76**, 165106 (2007).
[21] B. Gil, Phys. Rev. B **81**, 205201 (2010).
[22] B. Gil, B. Guizal, D. Felbacq, and G. Bouchitté, Eur. Phys. J. Appl. Phys **53**, 20303 (2011).
[23] P. Hohenberg and W. Kohn, Phys. Rev. **136**, B864 (1964).
[24] W. Kohn and L. J. Sham, Phys. Rev. **140**, A1133 (1965).
[25] M. Methfessel, M. van Schilfgaarde, and R. A. Casali, in *Electronic Structure and Physical Properties of Solids. The Use of the LMTO Method*, Lecture Notes in Physics, Vol. 535, edited by H. Dreyssé (Springer Verlag, Berlin, 2000), p. 114.
[26] T. Kotani and M. van Schilfgaarde, Phys. Rev. B **81**, 125117 (2010).
[27] L. Hedin, Phys. Rev. **139**, A796 (1965).
[28] H. Schulz and K. Thiemann, Solid State Commun. **23**, 815 (1977).

[29]M. Ueno, M. Yoshida, A. Onodera, O. Shimomura, and K. Takemura, Phys. Rev. B **49**, 14 (1994).
[30]E. Silveira, J. J. A. Freitas, M. Kneissl, D. W. Treat, N. M. Johnson, G. A. Slack, and L. J. Schowalter, Appl. Phys. Lett. **84**, 3501 (2004).
[31]J. Wu, W. Walukiewicz, W. Shan, K. M. Yu, J. W. Ager, E. E. Haller, H. Lu, and W. J. Schaff, Phys. Rev. B **66**, 201403 (2002).
[32]S. P. Fu and Y. F. Chen, Appl. Phys. Lett. **85**, 1523 (2004).
[33]A. V. Rodina, M. Dietrich, A. Göldner, L. Eckey, A. Hoffmann, A. L. Efros, M. Rosen, and B. K. Meyer, Phys. Rev. B **64**, 115204 (2001).
[34]L. Chen, B. J. Skromme, R. F. Dalmau, R. Schlesser, Z. Sitar, C. Chen, W. Sun, J. Yang, M. A. Khan, M. L. Nakarmi, J. Y. Lin, and H.-X. Jiang, Appl. Phys. Lett. **85**, 4334 (2004).
[35]E. Silveira, J. A. Freitas, O. J. Glembocki, G. A. Slack, and L. J. Schowalter, Phys. Rev. B **71**, 041201 (2005).
[36]B. Gil, O. Briot, and R.-L. Aulombard, Phys. Rev. B **52**, R17028 (1995).
[37]R. Goldhahn, P. Schley, A. Winzer, M. Rakel, C. Cobet, N. Esser, H. Lu, and W. Schaf, J. Cryst. Growth **288**, 273 (2006).
[38]W. R. L. Lambrecht, A. V. Rodina, S. Limpijumnong, B. Segall, and B. K. Meyer, Phys. Rev. B **65**, 075207 (2002).